

Article

Assessing the Critical Multifunctionality Threshold for Optimal Electrical, Thermal, and Nanomechanical Properties of Carbon Nanotubes/Epoxy Nanocomposites for Aerospace Applications

Aikaterini-Flora A. Trompeta ^{1,†}, Elias P. Koumoulos ^{1,†}, Sotirios G. Stavropoulos ^{2,†},
Theodoros G. Velmachos ^{2,†}, Georgios C. Psarras ^{2,†} and Costas A. Charitidis ^{1,*,†}

¹ Research Unit of Advanced, Composite, Nano-Materials & Nanotechnology, School of Chemical Engineering, National Technical University of Athens, Zographos, 15780 Athens, Greece; ktrompeta@chemeng.ntua.gr (A.-F.A.T.); elikoum@chemeng.ntua.gr (E.P.K.)

² Smart Materials & Nanodielectrics Laboratory, Department of Materials Science, University of Patras, 26504 Patras, Greece; Stavropoulos@upatras.gr (S.G.S.); teovelmachos@gmail.com (T.G.V.); psarras@upatras.gr (G.C.P.)

* Correspondence: charitidis@chemeng.ntua.gr; Tel.: +30-210-772-4046

† These authors contributed equally to this work.

Received: 17 December 2018; Accepted: 7 January 2019; Published: 10 January 2019



Abstract: Epoxy composites are widely used in primary aerospace structures, where high impact damage properties are necessary. However, challenges appear when multiple functionalities, including electrical and thermal conductivity, are needed in parallel with increased mechanical properties. The current study aims at the assessment of a critical concentration of multiwalled carbon nanotubes (MWCNTs), incorporated in epoxy resin, which will indicate a threshold for optimal electrical, thermal and mechanical properties. For the evaluation of this optimal concentration, electrical conductivity, thermal stability and nanomechanical properties (Young modulus and nanohardness) have been assessed, for epoxy nanocomposites with 0 to 15 parts per hundred resin per weight (phr) MWCNTs. Percolation theory was applied to study the electrical conductivity for different contents of MWCNTs in the epoxy nanocomposite system. Thermogravimetric analysis was employed for the assessment of the epoxy composites' thermal properties. Nanohardness and elastic modulus were measured, and the hardness versus modulus index was calculated. Emphasis was given to the dispersion of MWCNTs in the epoxy matrix, which was assessed by both microscopy techniques and X-ray micro-computed tomography. A correlation between the optimum dispersion and MWCNTs content in terms of electrical conductivity, thermal stability, and nanomechanical properties revealed a threshold concentration at 3 phr, allowing the manufacturing of aerospace structures with multifunctional properties.

Keywords: carbon nanotubes; electrical properties; multifunctionality; nanomaterials; nanomechanical properties; polymer nanocomposites; thermal stability; threshold concentration

1. Introduction

Nanocomposite materials combining a polymer with nanofillers have attracted research interest the last decades, due to the combined advantages they offer [1]. Carbon nanotubes (CNTs) have been widely used as nanofillers in epoxy composites, since they provide improved electrical, thermal, and mechanical properties in the final product [2]. The extraordinary properties of CNTs offer the ability to manufacture conducting polymers at low concentrations of the nanofiller, without altering the

performance of the polymer, in comparison with the use of other additives such as carbon black, which requires higher concentrations for an effective functionality [3]. Indeed, if the desired performance can be achieved at low concentrations, novel lightweight materials can be fabricated, to be used in a range of advanced applications. The benefits of composite materials are clearly depicted on aerospace applications which require lightweight, high-strength, high-stiffness, and highly fatigue-resistant materials [4]. The use of composites within the aerospace industry has revolutionized aircraft design, and has already resulted in significant fuel savings across many fleets (up to 20%) compared with aluminum. Composites have been used in aircraft parts, as presented in Table 1.

Table 1. Structural parts of aircrafts where composite materials can be used, according to Ghori et al., 2018 [5].

Primary Structural Parts	Secondary Structural Parts
Wings	Doors
Tails surfaces	Antenna dishes
Fuselages sections	Center wing boxes
Rocket motor castings	Landing gear doors
Engine nacelles and cowls	Floor beams
Horizontal and vertical stabilisers	Tall cones
Pressure bulkheads	Flap track panels

According to the above, the aerospace industry can exploit the extraordinary properties of CNTs to enhance the mechanical properties needed for aerospace constructions. Researchers have already studied the effect of CNTs on the mechanical properties of reinforced epoxy resin composites. Taraghi et al. studied the impact response for reinforced composites containing CNTs, and found that the impact strength can be increased up to 45% [6]. Several studies have also investigated the mechanical properties of such composites, focusing on the elasticity [7], tribology [8], toughness [9], and damage [10] of the specimens. Nanomechanical measurements through nanoindentation have also been used for the assessment of the mechanical properties of nanocomposites based on epoxy resin which have been reinforced with singlewalled CNTs (SWCNTs) [11], since nanomechanics are of great importance in the aeronautics and aerospace industry [12].

The aerospace industry can also benefit from the exploitation of cost-effective nanocomposite materials with tailored conductivity [13]. Carbon nanotubes have been distinguished from other nanomaterials, due to their extraordinary electrical and thermal properties. The study of Alsafee et al. [14] demonstrated the intrinsic potential of multiwalled carbon nanotubes (MWCNTs) to change the electrical behavior of an epoxy resin. It was revealed that a small quantity of MWCNTs can considerably modify the electrical properties, and transform the epoxy matrix from an insulator to a semiconductor. This finding can be exploited by the aerospace industry as a strategy for lightning strike protection [15]. Regarding the thermal properties, there is still a lot of space to investigate the connection between glass transition temperature and mechanical properties [16]. The aerospace industry is continuously working to develop lightweight and strong materials with increased thermal stability that can stand high temperatures [17].

Despite the fact that the above properties have individually been investigated extensively, combined studies aiming to assess a threshold concentration for the achievement of a transition in electrical and thermal properties together with an improvement in the nanomechanical properties for epoxy-based nanocomposites are really scarce. The work of Allaoui et al. [18] was an attempt to investigate electrical and mechanical properties, by means of tensile tests and AC/DC spectroscopy measurements. However, the mechanical testing had not been executed in the nanoscale to detect phenomena that are occurrent in such dimensions. Thus, this study, employing nanomechanical testing, thermal degradation evaluation, and electrical conductivity measurements, aims to meet the aforementioned properties and conclude on an optimum reinforcement concentration for the epoxy nanocomposite material, to be used in aerospace applications, as a nanomodified resin system of

the preparation of reinforced epoxy composites. In order to eliminate the chemical effects [11,19] and test the performance of the pristine MWCNTs, unmodified MWCNTs synthesized in-house have been chosen as nanofillers in this study. By this, the performance of existing masterbatches of epoxy resin with pristine CNTs that are commercially available and are potentially being used in aerospace applications will be assessed.

2. Materials and Methods

2.1. Materials

The chosen method for the synthesis of MWCNTs used in the preparation of the composites was thermal chemical vapor deposition (T-CVD). The supported catalyst approach was employed, as first reported in Trompeta et al.'s study [20], which offers higher productivity and yield, resulting in lower production costs (estimated at less than 1 euro/g). For the growth of MWCNTs, a catalyst containing Fe particles at 20 wt. % was synthesized in-house with the precipitation method, using a mix of zeolite and Al₂O₃ (50:50) as an absorbent substrate. Silicon (Si) wafers of N type, P doped, with a crystallographic orientation of (100) were used as substrate to deposit the catalyst prior its insertion in the reactor. The catalyst was placed on the polished side of the Si wafers, which were cut on the appropriate dimensions to fit inside the reactor, i.e., 3.4 × 10 cm. For each experiment, 0.3 to 0.8 g catalyst was used. Prior to the initiation of the experiment, purging with N₂ was necessary for 30 min to remove the oxygen from the reactor, and preheating at 550 °C took place for 1 h, for the calcination of the catalyst. Afterwards, the CVD reactor was heated up to 700 °C. Then, the reaction was started while feeding the system with acetylene with a volumetric flow of 100 mL/min. Simultaneously, the nitrogen flush was continued with a volumetric flow of 230 mL/min. The reaction for each batch lasted from 1 to 8 h. The product was received in a sponge-like form which was easily manipulated and turned into powder through mechanical grinding, to be used for the preparation of the nanocomposites. Each batch resulted in a production of ~6.5 g, which led to the repetition of the process for five times in order to obtain the necessary MWCNT quantity for the composites. Full repeatability was evident between the experiments, as can be seen in Figure 1, which depicts the morphology of the synthesized MWCNTs as received from two different batches. As it can be seen, both samples consisted of bundles of MWCNTs which varied in diameter from ~45 to 95 nm and had lengths of up to 5 μm, which classifies them as "short" MWCNTs [21].

Of all resins used in the aerospace industry, epoxy resins have gained the widest acceptance [22] since they offer versatility that is unattainable among other polymers, such as phenolic resins, polyurethanes, high-performance polymers (polyarylene ether nitrile (PEN) [23], addition-type polyimides (PI), i.e., polyamide-imide (PAI), polyphthalamide (PPA), polyethylenimine (PEI), polysulfones (PSU, PESU, PPSU), polyether ether ketone (PEEK), polyphenylene sulfide (PPS), polyvinylidene fluoride (PVDF), perfluoroalkoxy alkane (PFA), and liquid crystal polymers (LCP) [24]). Epoxy resins have a wide range of viscosities. Thus, they are adaptable to a wide variety of manufacturing processes. For example, filament winding and pultrusion using low-viscosity resins, or dry lay-up processing with solid-form resins [22]. The epoxy polymer matrix was prepared by mixing the low-viscosity (500–700 MPa·s) epoxy resin (Araldite® GY 257, based on Bisphenol A modified with an aromatic glycidyl ether), one of the most commonly used epoxy resins in aerospace applications [22], with hardener diethylenetriamine in a ratio of 1:0.05. This low-viscosity resin was chosen in order to avoid difficulties on the processability of the nanocomposites on high MWCNT content.

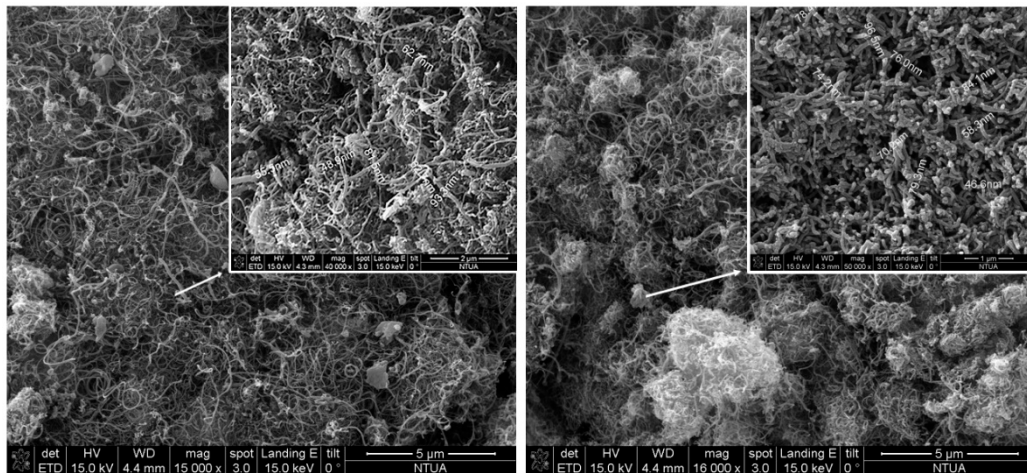


Figure 1. Entangled multiwalled carbon nanotubes (MWCNTs) with diameters ranging between 45 and 95 nm, used as nanofillers in the current study.

2.2. Composites Preparation

To prepare the composites, the entangled MWCNTs were first grinded through mechanical milling. Subsequently, the chosen quantity of MWCNT powder was added to the epoxy system, which included both the first part of the liquid epoxy resin and the hardener in a volume of 50 mL, in order to prepare admixtures with different concentrations of parts per hundred resin per weight (phr): 0.1 phr (sample EP01), 0.5 phr (sample EP05), 1 phr (sample EP1), 2 phr (sample EP2), 3 phr (sample EP3), 5 phr (sample EP5), 10 phr (sample EP10), and 15 phr (sample EP15). Higher loadings of up to 80 wt. % have been achieved with the procedure developed in the work of Schilde et al. [25]. However, the described procedure was out of the scope of the current study. The admixture was prepared via high-shear mechanical mixing, using a sawtooth impeller of 2 cm diameter, in 1000 rpm for 30 min for each sample, including the preparation of a bare resin sample reference for comparison reasons. According to the literature [26], high-shear mixing has proven to be more effective in comparison with other methods [27], such as ultrasonication, for the preparation of nanocomposites, since it enables the dispersion and intercalation of the nanofillers in the polymer matrix due to the temperature rise [28,29]. Despite the fact that this technique is not new, it can be considered cost- and time-effective, and it simulates the industrial production of polymer masterbatches, used in the polymer, paint, coatings, and composites industries [30]. The mixtures of each case were poured into small molds of 3 cm diameter, in duplicates, and were placed under vacuum overnight in order to absolve possible bubbles, since the first component of the resin system is a solution in a mono-functional reactive diluent. Afterwards, the composites were cured in a furnace at 70 °C for 4 days. The surface of the first replicate of each of the obtained specimens was grinded in order to be flattened, and one of the two sides was polished for the nanomechanical testing. For the electrical conductivity measurements, the second replicate was grinded from both sides, in order to obtain a disc-like specimen of about 2 mm thickness.

2.3. Characterization Techniques

2.3.1. Optical Microscopy

Optical microscopy was executed using an Axio Imager A.2m (Carl Zeiss MicroImaging GmbH, Jena, Germany) in the transmitted light configuration, using the bright field filter, in two magnifications ($\times 100$ and $\times 500$). Multiple images were acquired and combined (z-stitching) for high depth of field (DOF) images, using Zerene Stacker software (free trial version, Zerene Systems LLC, Richland, WA, USA).

2.3.2. Scanning Electron Microscopy

The morphologies of the MWCNTs used in this study, as well as the cryo-fractured surfaces of the nanocomposites (via liquid nitrogen), were examined by scanning electron microscopy (SEM) using a Nova™ NanoSEM 230 (FEI company, Hillsboro, OR, USA) microscope with a W (tungsten) filament, with all images acquired in secondary electron mode using an operating voltage of 15 kilovolts (kV).

2.3.3. X-ray Microcomputed Tomography (Micro-CT)

Micro-CT examination has been proven to be ideal for the study of reinforced composites, especially when their internal structures need to be assessed for demanding applications, such as aeronautics. Thus, the structures of the specimens were investigated by a compact desktop micro-CT, 3D X-ray scan system, SkyScan 1272 (Bruker, Kontich, Belgium). The system consisted of a microfocus sealed X-ray source L11871-02 (Hamamatsu Photonics K.K, Hamamatsu, Japan) which operated at 20–100 kV and 10 W (< 5 µm spot size @ 4 W). The X-ray detector, which had a resolution of 11 Mp (4032 × 2688 pixels) was coupled to the scintillator. The distance between the rotation axis and the radiation source was set from 6 to 12 mm, and the pixel resolution was set to 2016 × 1344 in order to obtain reliable images. The X-ray tube voltage was set to 40 kV and the X-ray tube current was set to 250 µA for all the specimens. After the acquisition of the X-ray projection images, the 3D image was reconstructed by the image processing software of the X-ray CT system (InstaRecon®, Bruker, Kontich, Belgium).

2.3.4. Electrical Measurements

Electrical measurements were conducted by means of Broadband Dielectric Spectroscopy (BDS) in a wide frequency (10^{-1} – 10^6 Hz) and temperature range (30–150 °C), via an Alpha-N Analyzer, high resolution dielectric analyzer (Novocontrol Technologies & Co. KG, Montabaur, Germany). The applied voltage amplitude was 1 V in all cases. Examined specimens were put, in a parallel plate form, in the BDS 1200 dielectric cell and subjected to isothermal scans with a temperature step of 10 °C. Temperature was controlled via a Novotherm system, and real-time data acquisition was performed by employing Windeta software (Novocontrol Technologies & Co. KG, Montabaur, Germany). The software, dielectric cell, and temperature control system were also supplied by Novocontrol Technologies.

2.3.5. Thermogravimetric Analysis

Thermal properties were examined using a STA 449F5 Jupiter® thermogravimetric analyzer (Netzsch, Selb, Germany) in a temperature range from 25 to 1000 °C, under a constant air flow of 50 mL/min, while heating rate was set to 10 °C per minute.

2.3.6. Nanomechanical Assessment

Through their responses to local loading, the nanomechanical integrities of the materials were assessed through a Hysitron (Minneapolis, MN, USA) TriboLab® Nanomechanical Test Instrument, which recorded the displacement with a load resolution of 1 nN and displacement resolution of 0.04 nm. In all presented data, a total of 10 indents were performed so as to determine the average hardness (H) and elastic modulus (E) values, with spacing of 50 µm, at room temperature with 45% humidity. The closed-loop feedback control option was selected. All measurements were performed using the standard three-sided pyramidal Berkovich diamond tip indenter (radius of 100 nm) [31,32].

From the half-space elastic deformation theory, H and E values were extracted from the experimental data (load–displacement curves) using the Oliver-Pharr (O&P) model [33]. The expressions that calculate E , extracted from load–displacement curves, are based on Sneddon's [34] elastic contact theory:

$$E_r = \frac{S\sqrt{\pi}}{2\beta\sqrt{A_c}} \quad (1)$$

where S is the unloading stiffness (initial slope of the unloading load–displacement curve at the maximum displacement of penetration (or peak load)), A_c is the projected contact area between the tip and the substrate, and β is a constant that depends on the geometry of the indenter ($\beta = 1.167$ for the Berkovich tip [33,34]). Nanoindentation H refers to the mean contact pressure required. This hardness, which is the contact hardness (H_c), is actually dependent upon the area geometry of the tip indenter, as described in Equations (2)–(4):

$$H_c = F/A \quad (2)$$

where

$$A(h_c) = 24,5h_c^2 + a_1h_c + a_{1/2}h_c^{1/2} + \dots + a_{1/16}h_c^{1/16} \quad (3)$$

and

$$h_c = h_m - \varepsilon \frac{P_m}{S_m} \quad (4)$$

where h_m is the total penetration displacement of the indenter at peak load, P_m is the peak load at the indenter displacement h_m , and ε is an indenter geometry constant, equal to 0.75 for the Berkovich indenter [32–35]. Prior to indentation, the area function of the indenter tip was calibrated in a fused quartz/silica (standard material) [36].

3. Results and Discussion

3.1. Dispersion Characterization

In order to fully exploit the properties of CNTs and to transfer the mechanical, electrical, and thermal stability enhancements to the polymer matrix, an effective dispersion should be achieved [37]. A strong interfacial bonding between the inorganic phase of the CNTs and the organic phase of the polymer is the main challenge for the formation of successful polymer nanocomposites. To achieve this prerequisite, a homogenous dispersion of CNTs in the matrix is also important [38]. However, the entanglement of CNTs leads to agglomeration in the micrometer scale [39]. The following results, retrieved from advanced microscopy techniques and micro-CT, prove the effectiveness of the CNT dispersion in the epoxy matrix [40].

3.1.1. Optical Microscopy

For the evaluation of the dispersion of MWCNTs in the epoxy resin, optical microscopy was chosen for an initial assessment [19]. From the prepared samples, the transparent one was chosen (EP01: 0.1 phr MWCNTs) for observation in the transmittance mode. The results are depicted in Figure 2, in two different magnifications ($\times 100$ and $\times 500$, respectively). As it can be seen, MWCNT bundles were homogeneously dispersed within the epoxy matrix. Agglomerates of about 30–50 μm were observed, and they can improve the impact resistivity of the composites since they can absorb the energy from the stress.

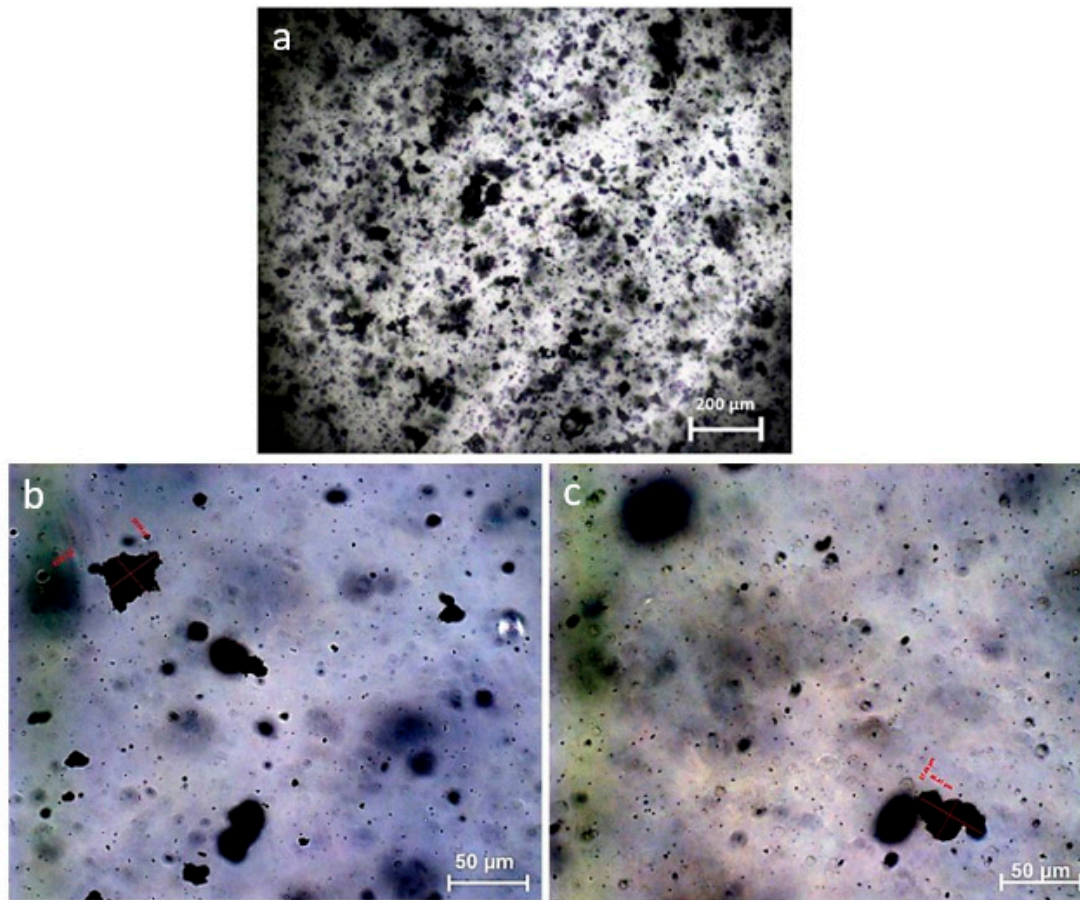
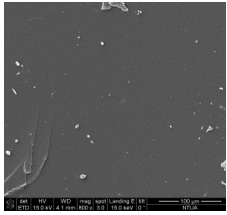
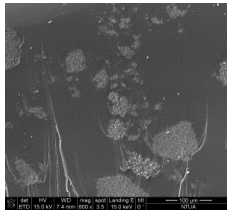
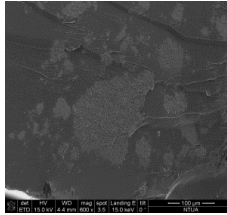
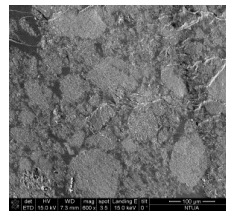
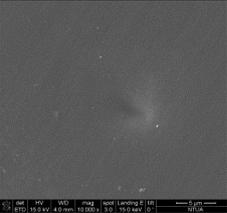
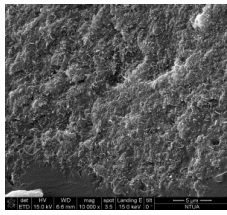
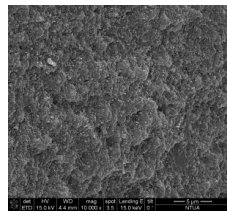
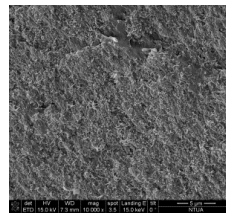
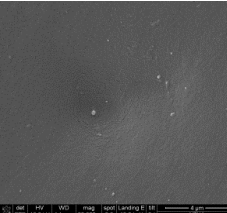
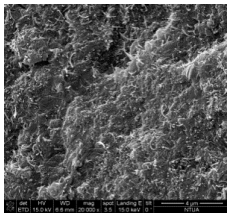
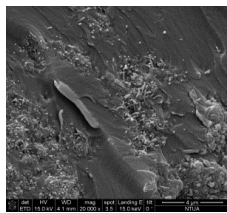
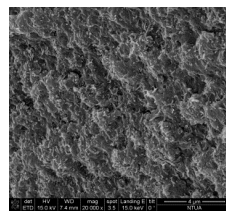
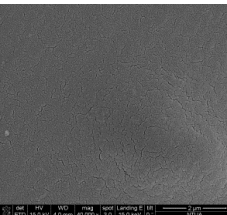
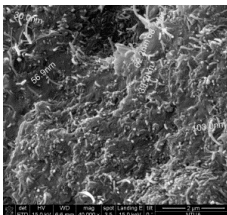
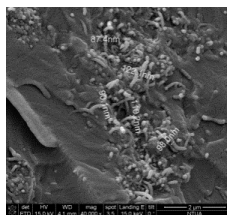
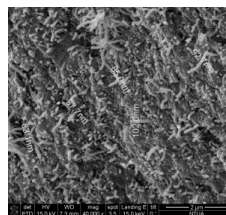


Figure 2. (a) Optical microscopy image (transmittance mode) for EP01 where the dispersion of MWCNTs is observed; magnification: $\times 100$); (b and c) Optical microscopy image (transmittance mode) for EP01 at $\times 500$ magnification. The dimensions of the MWCNT bundles are up to $\sim 30 \mu\text{m}$.

3.1.2. Study of Cryo-Fractured Surface

The cryo-fractured surfaces of three indicative samples with a low (0.5 phr), medium (3 phr), and high (15 phr) concentration were studied under SEM, and the results are shown in Table 2. In the low magnification ($\times 600$), it was possible to have an estimation of the dispersion of MWCNTs inside the composite. It is clear that the low concentration does not enable the existence of MWCNTs in every part of the specimen. On the other hand, when the concentration increased, MWCNTs were uniformly dispersed in the whole matrix. Also, the fracture lines were evident in the low magnifications. It could be observed that the fracture lines are blocked around the MWCNT areas, as shown for the EP05 and EP3 samples. In this case, MWCNT agglomerates work as barriers for the crack propagation. In higher magnifications ($\times 10,000$, $\times 20,000$), the structure of MWCNT agglomerates and the alignment of the MWCNTs in the polymer matrix could be observed. Finally, the magnification of $\times 40,000$ enabled the observation of MWCNTs as well as their dimensioning. It may be remarked that the observed diameters of MWCNTs inside the composite were slightly increased (MWCNTs seem to become thicker) in comparison with the measured diameters that are presented in Figure 1. This indicates that the polymer has been wrapped around MWCNTs with non-covalent bonds.

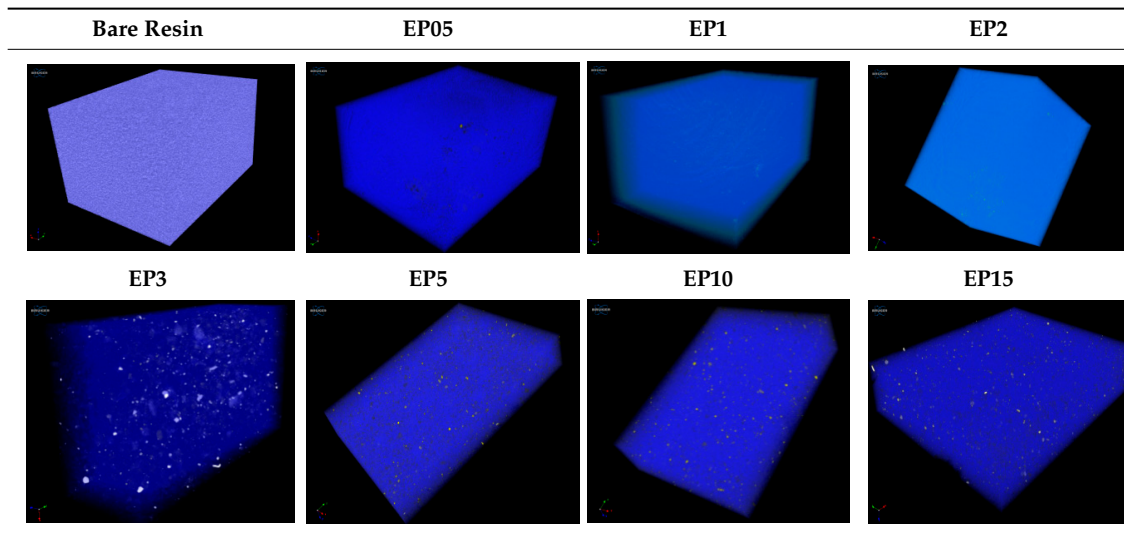
Table 2. SEM images of the cryo-fractured surfaces of the nanocomposites.

Mag.	Bare Resin	EP05	EP3	EP15
×600				
×10,000				
×20,000				
×40,000				

3.1.3. Evaluation of Dispersion through Micro-CT

According to Kim et al. [37], the actual dispersion of nanofillers within polymer composites cannot be easily evaluated using SEM. On the contrary, the real dispersion could be clearly observed in the 3D micro-CT images. Thus, in Table 3, the dispersion of MWCNTs in selected samples is depicted, after the micro-CT scanning. In each case, a cuboid representative volume that was considered to be representative of the entire volume was identified for detailed analysis. As it can be seen, for concentrations of up to 2 phr, the dispersion of MWCNTs in the epoxy matrix was too sparse. However, for concentrations of 3 phr and higher, a homogenous dispersion could be achieved, covering the entire volume of the specimen. Thus, a network can be formatted, as possible conjunctions are feasible. Moreover, micro-CT was implemented in order to assess the structural integrity of the samples and the detection of possibly remaining voids that occurred during the degassing process. After the examination of all samples, it could be remarked that voids were not detected, as they would have been marked with a different color (red) due to their density difference with the epoxy resin and the MWCNTs.

Table 3. Microcomputed Tomography (Micro-CT) images of MWCNT–epoxy samples.



3.2. Electrical Conductivity Evaluation

In Figure 3, the AC conductivity at two different temperatures is shown as a function of the applied frequency for nanocomposites and neat epoxy. AC conductivity was evaluated from the dielectric loss factor (ϵ'') via Equation (5):

$$\sigma_{AC} = \epsilon_0 \omega \epsilon'' \tag{5}$$

where ϵ_0 is the permittivity of free space and ω is the angular frequency of the applied field.

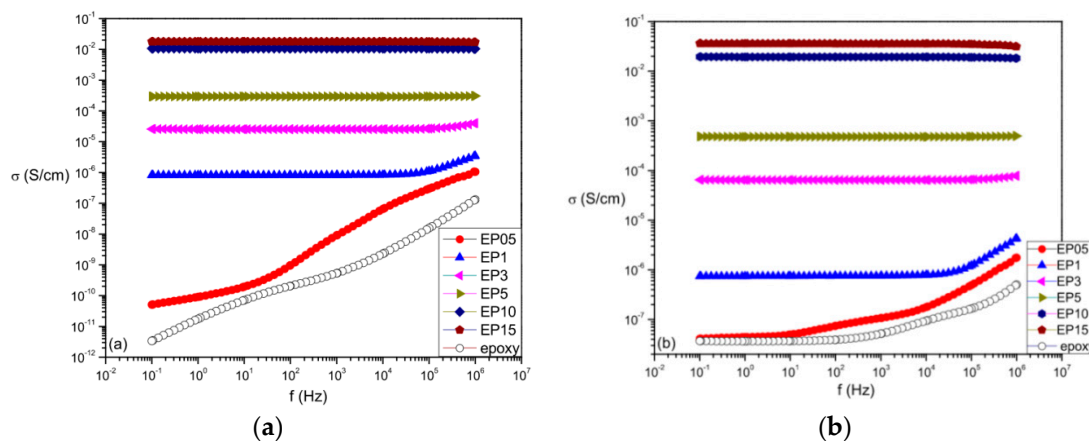


Figure 3. Variation of conductivity with frequency at: (a) 30 °C and (b) 90 °C.

Conductivity values increase with filler content, while being temperature- and frequency-dependent. In the study of Bellucci et al., the resistivity of epoxy resin with 0.5 wt. % CNTs with similar geometrical characteristics as in our study was tested, and a reduction 10^3 was found [38]. In our case, the neat epoxy and EP05 specimens exhibited a dispersion of conductivity with frequency. At low frequencies, σ_{AC} values tended to be constant, approaching their DC conductivity value, whereas after a characteristic frequency, conductivity followed an exponential dependence. In the low-frequency regime, the applied electric field keeps its direction for a longer time compared to the high-frequency regime, thus allowing charge carriers to migrate longer distances within the material. However, the insulating nature of the matrix exerts strong restrictions to this motion, diminishing the number of carriers which are able to overcome the existing potential barriers. Therefore, a limited

number of charge carriers migrate at relatively longer distances. At the high-frequency region, the alternation of the field does not provide sufficient time for charge carriers to migrate at relatively long distances. On the other hand, charges are able to move or hop between adjacent conductive sites. The outcome of this process is increased values of conductivity, since a large number of charges participate by hopping between neighboring positions, covering very short distances [39,40]. At higher temperatures, the dispersion of conductivity with frequency decreases, because thermal agitation facilitates the migration of charge carriers, as shown in Figure 3b. This facilitation is also expressed via the enhanced values of conductivity.

Concerning the effect of MWCNT content, an abrupt increase of conductivity, of several orders of magnitude, was observed for the specimen EP3, with 3 phr MWCNT content, over the whole frequency and temperature range. This increase, in the case of 0.1 Hz and 30 °C, exceeded the seven orders of magnitude, providing a strong indication that the examined nanocomposites underwent a transition from insulating to conductive behavior. Moreover, the influence of frequency upon conductivity values vanished with increasing MWCNT content, and apparently became negligible for concentrations higher than 1 phr, implying that the critical concentration for the transition from insulating to conductive behavior lies between 1 and 3 phr filler content. This is also in agreement with [19]. The insulator-to-conductor transition is considered as a critical phenomenon, and can be described by means of percolation theory according to Equation (6):

$$\sigma \approx (P - P_C)^t \quad (6)$$

where P is the content of the conductive phase, P_C the critical concentration (also known as the percolation threshold), and t is a critical exponent related to the dimensionality of the conduction process [39,40]. At the critical concentration, a conductive path is formed, allowing charge carriers to migrate through the whole nanocomposite [41].

The variation of conductivity with MWCNT content and frequency at two temperatures is depicted in the plots of Figure 4.

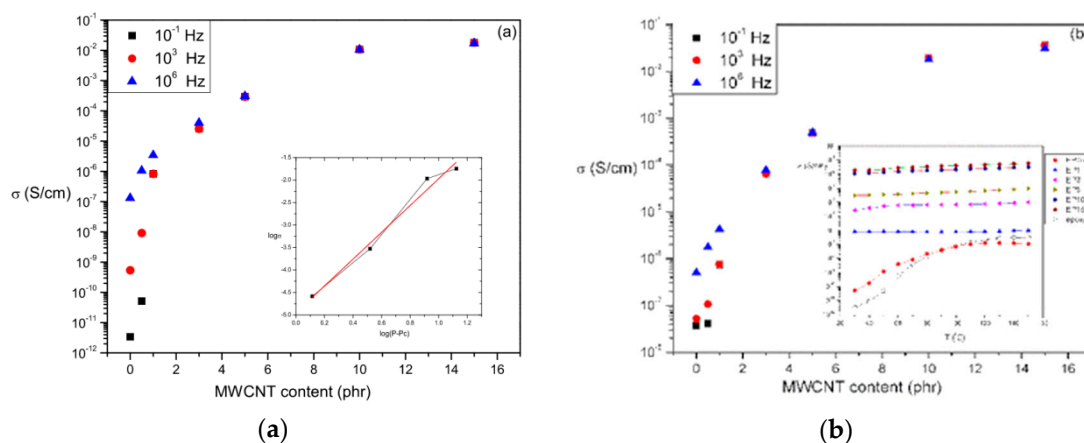


Figure 4. Variation of conductivity with MWCNT content and frequency at: (a) 30 °C (the inset provides an example of percolation threshold determination), and (b) 90 °C (the inset depicts the variation of conductivity with temperature at $f = 0.1$ Hz).

It can be observed that, within a narrow variation of filler content, a significant alteration of conductivity exists in all cases. The effect of temperature is more pronounced at low frequencies and below the critical concentration, since the low alternation of the field and the thermal agitation provide sufficient time and energy for charge carriers to migrate within the nanocomposite. Fitting the experimental data with Equation (6) in its double logarithmic form allowed for the determination of the critical concentration and exponent, which in the case of 0.1 Hz and 30 °C were 1.7 and 2.8,

respectively. The determined value of the percolation threshold confirmed that the EP3 nanocomposite had undergone the insulating-to-conductive transition, while the value of the critical exponent appeared to exceed the value predicted by classical percolation theory, which for a three-dimensional conduction process is two. Deviations from the predicted value by classical percolation theory are often observed, and can be attributed to the differences between a perfect lattice with spherical conductive inclusions having no mutual interactions, and a real CNT-polymer system. The dynamic nature of the nanocomposite, along with interactions between the conductive MWCNTs and the composite's phases, contribute to this discrepancy [39–41].

As illustrated in Figure 3, the shapes of the recorded spectra of conductivity as a function of frequency, especially for the neat epoxy and EP05 systems, imply hopping conductivity as the dominating conductance mechanism [26,41]. The situation changes above the percolation threshold, where the effect of frequency upon conductivity values diminishes rapidly. At filler concentrations higher than the critical one, a conductive path (or paths) is created within the specimens, through which carriers can percolate the whole sample. Thus, another conduction mechanism occurs, and conduction is carried out via the geometrical contacts of MWCNTs in the path or paths. The inset of Figure 4b depicts the dependence of conductivity on temperature, at a constant frequency of 0.1 Hz, for the same set of specimens. Interestingly, the influence of temperature below and above the percolation threshold, as expressed by the differential $d\sigma/dT$, changed. Below the critical concentration, $d\sigma/dT$ is positive and conductivity values increased, indicating the dielectric/insulating nature of the composites. At these low filler contents, conductive paths are incomplete and charges are migrating via hopping conductivity. Above the critical concentration, $d\sigma/dT$ decreased approaching zero, since conduction via the created paths came into play. It should be noted that in the cases where metallic-type conduction takes place, the sign of $d\sigma/dT$ becomes negative. The absence of negative values of the differential $d\sigma/dT$ in the recorded data suggested that metallic-type conduction was not the dominating process, and hopping conductivity also appeared above the percolation threshold.

3.3. Thermal Decomposition Evaluation

Figure 5 shows TGA curves of the bare epoxy and MWCNT/epoxy composites from 380 to 520 °C in air atmosphere, which is the focus-of-interest range from the full TGA curves, where the thermal degradation phenomena take place. The thermal decomposition profile of the bare epoxy resin consisted of a drastic weight loss at around 360 °C, which corresponds to the degradation of bisphenol A groups [42]. In principle, MWCNTs showed good thermal stability as reinforcing agents, with a decomposition temperature of around 520 °C. They were completely decomposed at around 690 °C [43]. This good thermal stability is attributed to the high crystallinity of MWCNTs, due to their graphitic structure. This resulted in a higher thermal stability of the epoxy composite as the content of MWCNT increased, which is in accordance with the study of Si-Eun et al [44]. For a specific temperature, the weight loss of the composites with higher MWCNT phr was lower. Moreover, two distinct regions can be observed: The first one includes the lower concentrations of 0.1 to 2 phr content, while the second one refers to higher concentrations of 3 to 10 phr content. It may be remarked that the thermal stability increased three times in comparison to the bare resin with the 3 phr content, which is a threshold that comes in accordance with the electrical conductivity measurements. Finally, it should be mentioned that the difference observed in the inset graph at 200 °C, which corresponds to the bare resin (black squares), is a typical behavior of epoxy resins, which is attributed to moisture loss and entrapped solvent remaining in the sample, according to Baldissera et al. [45].

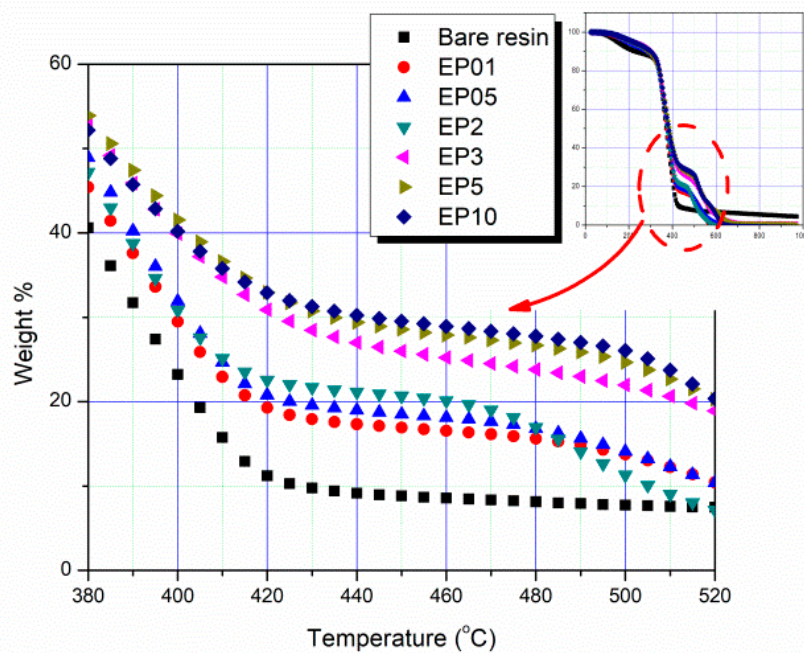


Figure 5. Thermogravimetric curves of nanocomposites.

3.4. Nanomechanical Characterization

Nanomechanical testing can overcome obstacles that are evident in the case of traditional mechanical measuring methods, such as tensile tests and microhardness testing. In parallel, the study of the local mechanical properties in a small volume can be achieved through nanoindentation, taking into account the material's microstructural gradients. The tiny contact area between the indenter and the sample's surface leads to high stress under specific loads. At low loads, a very prominent phenomenon is the so-called "Indentation Size Effect" (ISE), due to imperfection in tip geometry. This effect may cause deviations in the accurate measurement of hardness values [46].

Prior to nanoindentation and in order for the areas selected for being probed to be considered adequate (i.e., representative of the sample and of low roughness), the surfaces of the nanocomposites had been carefully examined (also for selection purposes) through Scanning Probe Microscopy (SPM) imaging ($70\ \mu\text{m} \times 70\ \mu\text{m}$). Representative images, together with the roughness assessments, are presented in Figure 6.

Hardness and modulus values were found to deviate at surface regions ($\sim 0\text{--}400\ \text{nm}$), probably due to the roundness of the tip and ISE, tending to reach constant values as shown in Table 4.

The graded surface structures due to the existence of MWCNTs, as well as the MWCNT bundling, can be considered as possible contributors to the wide range of hardness and modulus values obtained from the nanoindentation measurements. In parallel, the adhesive forces between the tip and the sample also affected the nanoindentation results. Improved nanomechanical properties were revealed for the cases of all samples, except for samples EP5 and EP10 which exhibited decreasing H and E values, leading to significantly lower nanomechanical properties values, indicating deterioration. This is illustrated in Figure 7. When comparing with other concentrations, the case of EP3 was the optimal concentration threshold that strengthened the epoxy matrix.

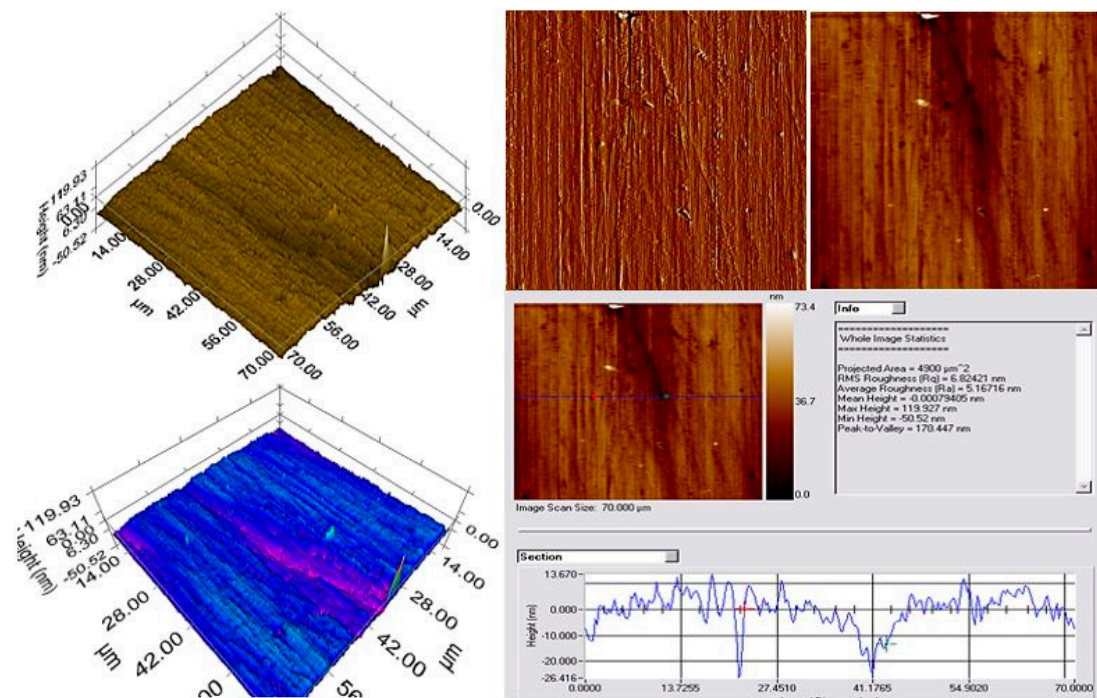


Figure 6. Representative SPM imaging of all samples, together with roughness assessments.

Table 4. Hardness and modulus bulk values of MWCNT-epoxy samples.

Sample	Hardness (<i>H</i>) (MPa)	Elastic Modulus (<i>E</i>) (GPa)
EP01	60 ± 3	0.8 ± 0.4
EP05	80 ± 3	2.0 ± 0.1
EP1	80 ± 4	2.0 ± 0.2
EP2	90 ± 5	2.0 ± 0.1
EP3	140 ± 6	2.4 ± 0.1
EP5	50 ± 4	0.7 ± 0.1
EP10	40 ± 3	0.5 ± 0.1
EP15	140 ± 5	2.0 ± 0.1

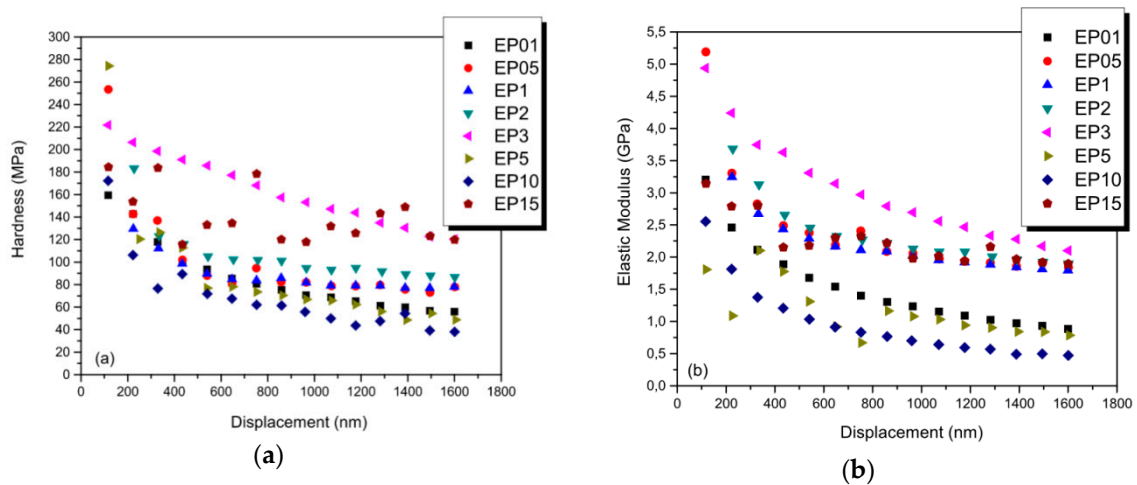


Figure 7. Nanomechanical properties, namely (a) hardness and (b) modulus, of nanocomposite samples.

As it can be seen, a low concentration of MWCNTs in the epoxy matrix provides a satisfying interfacial interaction that leads to the stretching of the epoxy molecules which have been attached to the MWCNTs, as also proven by the SEM cross-sectional analysis of the cryo-fractured surfaces. Additionally, a tube–tube slip can occur in the individual MWCNT rich-phase clusters. As MWCNT concentration was increased (EP01 to EP3 sample), there was a large increase in the stiffness of the system, which resulted in a reduction in the energy dissipated during the experiment. However, there were more tube–tube slips in the system at higher concentrations, since percolation, coupled to a better dispersion, leads to a higher contact surface among MWCNTs. For the EP5, EP10, and EP15 samples, dissipated energy increased—increased elasticity is also evidenced in Figure 8a, but with increased deviation relating with dispersion.

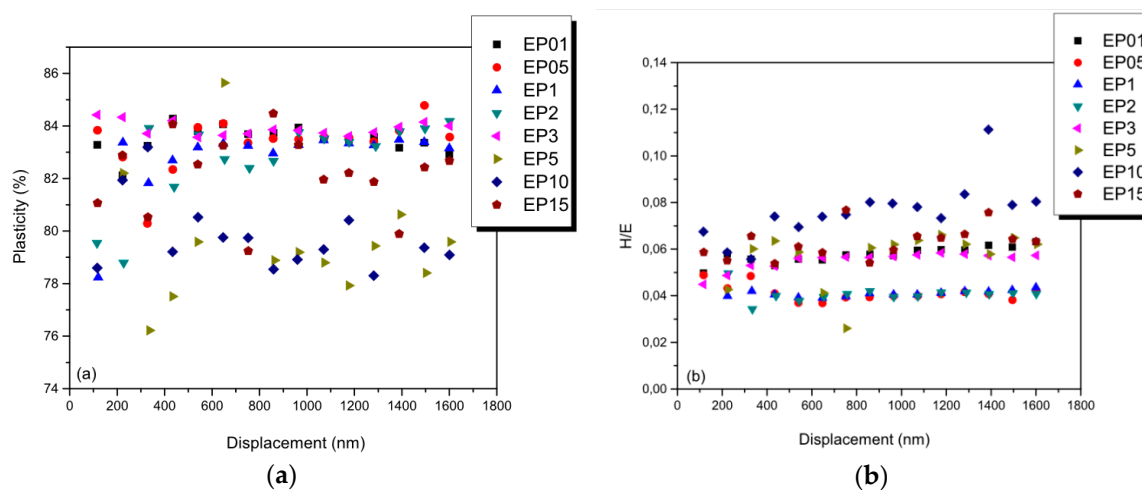


Figure 8. (a) Plasticity index obtained from load–unload curve area calculation, and (b) hardness-to-modulus ratios as indexes of resistance to wear.

It has been observed that the mechanical properties tend to deteriorate with increasing MWCNT content, after the threshold concentration of 3 phr. This fact is attributed to an extensive tube–tube slip mechanism, while nanotube contacts are unavoidable because of the sticky inter-particle tendency. Thus, these contacts (acting as knots) give rise to micron-sized agglomerates acting as mechanical defects for the resulting composite [47–49].

To evaluate the tribological properties of the nanocomposites, the hardness/elastic modulus ratio (H/E) has been calculated. The high values of the ratio are expected at higher stresses (usually evident in hard materials), whereas a low H/E indicates lower stresses which are distributed in the cross-section of the composite (found in softer materials) [50]. When H/E is high, a good wear resistance can be achieved [51,52], which has also been proven for polymeric materials. In Figure 8b, a change in the H/E slope is evident. This deviation reveals the strengthening of the nanocomposite with the addition of a critical amount MWCNTs. On the other hand, lower deviation of H/E values can prove the good dispersion of the MWCNTs in the polymer, with an almost-stable behavior at resistance to wear.

4. Conclusions

The potential use of MWCNT/epoxy nanocomposites in aerospace applications was investigated in this study, taking into account the main properties that are important for the materials choice in such constructions. The intrinsic potential of MWCNTs to considerably modify the mechanical and electrical behaviors of a polymer matrix, in low contents, was evident. MWCNTs in a content of 3 phr managed to improve the performance of epoxy composites, in terms of mechanical properties, thermal stability, and electrical conductivity, without the need of any further chemical process. The main findings

summarized below are consistent with the formation of a MWCNT network over the percolation threshold, leading to MWCNT slipping:

- From the optical microscopy in transmittance mode, it could be observed that MWCNT bundles were homogeneously dispersed within the epoxy matrix for the samples with low MWCNT content. From the SEM analysis it was proven that when the concentration increased, MWCNTs were uniformly dispersed in the whole matrix. Finally, from the micro-CT it was evident that for MWCNT contents of 3 phr and higher, a homogeneous dispersion could be achieved, covering the entire volume of the specimen.
- Conductivity increased with MWCNT content, and at a critical concentration it raised abruptly up to seven orders of magnitude, signifying the transition from the insulating to conductive behavior. Through thermogravimetric analysis, the thermal stability was showed to increase with increasing MWCNT content.
- Variations in conductivity with filler content can be studied in terms of percolation theory, and the determined percolation threshold and critical exponent, at 0.1 Hz and 30 °C, were 1.7 and 2.8, respectively.
- EP3 exhibited improved nanomechanical properties, while increasing concentration further revealed decreasing H and E values. The dispersion of MWCNTs has a great impact on nanomechanical properties, and should be taken into consideration.
- There was a large increase in the stiffness of the system, which resulted in reducing the energy dissipated during the experiment. However, there was more tube–tube slip in the system at higher concentrations, since percolation, coupled to a better dispersion, leads to a higher contact surface among MWCNTs. For the EP5, EP10, and EP15 samples, the dissipated energy increased.
- There was considerable improvement in the wear resistance due to the addition of MWCNTs. Moreover, lower deviation of H/E values revealed the good dispersion in the matrix, with impacts in almost-stable behavior at resistance to wear.

To achieve a better compatibility between MWCNTs and the epoxy matrix, avoiding the formation of agglomerates, and possibly lowering the MWCNT content in the nanocomposite, future work will be focused on the use of MWCNTs with an appropriate surface functionalization. The results can be compared with the main findings of this study, in order to investigate the effect of MWCNT functionalization on the electrical, thermal, and mechanical responses of the nanocomposites for self-sensing applications that can be applied in aerospace. However, this study proved that despite the fact that MWCNTs have not undergone any functionalization or purification process, they can modify the properties of an epoxy resin at a critical concentration, which is a multifunctionality threshold. By this, aerospace structures can be developed using carbon fiber-reinforced composites with MWCNT/nanocomposite epoxy resin, which can lead to enhanced electrical, thermal, and mechanical properties.

Author Contributions: Conceptualization, E.P.K.; methodology, A.-F.A.T., E.P.K., S.G.S., T.G.V.; investigation, A.-F.A.T., E.P.K., S.G.S., T.G.V.; formal analysis, E.P.K., S.G.S., T.G.V.; visualization, A.-F.A.T., E.P.K.; writing—original draft preparation, A.-F.A.T.; writing—review and editing, E.P.K., G.C.P., C.A.C.; supervision, G.C.P. and C.A.C.; project administration, C.A.C.; funding acquisition, C.A.C.

Funding: This research was funded by European Union's Horizon 2020 Research and Innovation Programme MODCOMP (Modified cost effective fibre-based structures with improved multi-functionality and performance), under grant number 685844.

Conflicts of Interest: The authors declare no conflict of interest.

References

1. Tjong, S.C. Structural and mechanical properties of polymer composites. *Mater. Sci. Eng. R Rep.* **2006**, *53*, 73–197. [CrossRef]
2. Thostenson, E.T.; Chou, T.W. Processing–structure multifunctional property relationship in carbon nanotube/epoxy composites. *Carbon* **2006**, *14*, 3022–3029. [CrossRef]
3. Zhang, H.; Zhang, Z.; Zhao, G.; Liu, Y. Influence of carbon black with different concentration on dynamic properties and heat buildup of semi-efficient natural rubber composites. *Micro Nano Lett.* **2016**, *11*, 402–406. [CrossRef]
4. Quilter, A. Composites in Aerospace (White Paper). Available online: https://ihsmarkit.com/pdf/Composites-Aerospace-Applications-whitepaper_264558110913046532.pdf (accessed on 29 December 2018).
5. Ghorri, S.W.; Siakeng, R.; Rasheed, M.; Saba, N.; Jawaaid, M. The role of advanced polymer materials in aerospace. In *Sustainable Composites for Aerospace Applications*; Woodhead Publishing Series in Composites Science and Engineering; Woodhead Publishing: Sawston, UK, 2018; pp. 19–34.
6. Taraghi, I.; Fereidoon, A.; Mohyeddin, A. The effect of MWCNTs on the mechanical properties of woven Kevlar/epoxy composites. *Steel Compos. Struct.* **2014**, *17*, 825–834. [CrossRef]
7. Selmi, A.; Friebel, C.; Doghri, I.; Hassis, H. Prediction of the elastic properties of single walled carbon nanotubes reinforced polymers. *Compos. Sci. Technol.* **2007**, *67*, 2071–2084. [CrossRef]
8. Giraldo, L.F.; Lopez, B.L.; Bostow, W. Effect of the type of carbon nanotubes on tribological properties of polyamide. *Polym. Eng. Sci.* **2009**, *49*, 896–902. [CrossRef]
9. Gojnya, F.H.; Wichmann, M.H.G.; Köpke, U.; Fiedler, B.; Schulte, K. Carbon nanotube reinforced epoxy composites: Enhanced stiffness and fracture toughness at low nanotube content. *Compos. Sci. Technol.* **2004**, *15*, 2363–2371. [CrossRef]
10. Kao, C.C.; Young, R.J. Assessment of interface damage during the deformation of carbon nanotubes composites. *J. Mater. Sci.* **2010**, *45*, 1425–1431. [CrossRef]
11. Lagoudas, D.C.; Piyush, R.; Thakre, A.; Benzerger, A. *Nanoindentation of CNT Reinforced Epoxy Nanocomposites*; Department of Aerospace Engineering, Texas A & M University: College Station, TX, USA, 2012.
12. Tan, B. Nanomechanics: Aeronautics and Aerospace Prospective. *J. Aeronaut. Aerosp. Eng.* **2012**, *1*, 117. [CrossRef]
13. Sandler, J.K.W.; Kirk, J.E.; Kinloch, L.A.; Shaffer, M.S.P.; Windle, A.H. Ultralow electrical percolation threshold in carbonnanotube epoxy composites. *Polymer* **2003**, *44*, 5893–5899. [CrossRef]
14. Alsafee, A.B.; Al Ajaj, I.A.; Khalil, A. Electrical conductivity of untreated multiwalled carbon nanotube/epoxy composites. *Int. J. Appl. Innov. Eng. Manag.* **2014**, *3*, 22–31.
15. Logakis, E.; Skordos, A.A. Lightning strike performance of carbon nanotube loaded aerospace composites. In Proceedings of the ECCM15—15th European Conference on Composite Materials, Venice, Italy, 24–28 June 2012.
16. Allaoui, A.; El Bounia, N. How carbon nanotubes affect the cure kinetics and glass transition temperature of their epoxy composites?—A review. *Express Polym. Lett.* **2009**, *3*, 588–594. [CrossRef]
17. Meador, M.A. High temperature polymer matrix composites. In *Aeropropulsion '87*; Session 1: Aeropropulsion Materials Research; NASA Lewis Research Center: Cleveland, OH, USA; p. 15.
18. Allaoui, A.; Bai, S.; Cheng, H.; Bai, J. Mechanical and electrical properties of a MWNT/epoxy composite. *Compos. Sci. Technol.* **2002**, *62*, 1993–1998. [CrossRef]
19. Lillehei, P.T.; Kim, J.-W.; Gibbons, L.J.; Park, C. A quantitative assessment of carbon nanotube dispersion in polymer matrices. *Nanotechnology* **2009**, *20*, 325708. [CrossRef]
20. Trompeta, A.F.; Koklioti, M.A.; Perivoliotis, D.K.; Lynch, I.; Charitidis, C.A. Towards a holistic environmental impact assessment of carbon nanotube growth through chemical vapour deposition. *J. Clean. Prod.* **2016**, *129*, 384–394. [CrossRef]
21. Zhou, H.; Han, G.; Xiao, Y.; Chang, Y.; Zhai, H.-J. A comparative study on long and short carbon nanotubes-incorporated polypyrrole/poly(sodium 4-styrenesulfonate) nanocomposites as high-performance supercapacitor electrodes. *Synth. Mater.* **2015**, *209*, 405–411. [CrossRef]
22. May, C.A. Resins for Aerospace. *Appl. Polym. Sci.* **1985**, *285*, 557–580. [CrossRef]
23. Wei, R.; Tu, L.; You, Y.; Zhan, C.; Wang, Y.; Liu, X. Fabrication of crosslinked single-component polyarylene ether nitrile composite with enhanced dielectric properties. *Polymer* **2018**, *161*, 162–169. [CrossRef]

24. High Performance Polymers in the Aerospace and Automotive Sectors, Frost and Sullivan. Available online: <https://store.frost.com/high-performance-polymers-in-the-aerospace-and-automotive-sectors.html#section1> (accessed on 29 December 2018).
25. Schilde, C.; Schlomann, M.; Overbeck, A.; Linke, S.; Kwade, A. Thermal, mechanical and electrical properties of highly loaded CNT epoxy composites: A model for the electric conductivity. *Compos. Sci. Technol.* **2015**, *117*, 183–190. [[CrossRef](#)]
26. AlQadhi, M.; Merah, N.; Khan, Z.; Mezghani, K.; Gasem, Z.; Adinoyi, M.J. Effect of sonication and high shear mixing parameters on nanoclay dispersion in epoxy. In Proceedings of the ECCM15—15th European Conference on Composite Materials, Venice, Italy, 24–28 June 2012.
27. Liu, C.-X.; Choi, J.W. Improved Dispersion of Carbon Nanotubes in Polymers at High Concentrations. *Nanomaterials* **2012**, *2*, 329–347. [[CrossRef](#)] [[PubMed](#)]
28. AlQadhi, M.; Merah, N. Method for Preparation of Epoxy Clay Nanocomposites. U.S. Patent 9334387B2, 10 September 2013.
29. Huang, Y.Y.; Ahir, S.V.; Terentjev, E.M. Dispersion rheology of carbon nanotubes in a polymer matrix. *Phys. Rev. B* **2006**, *73*, 125422. [[CrossRef](#)]
30. Berkovich, A.R.; Hower, J.C.; Jacques, D.; Rantell, T. Fabrication of Carbon Multiwall Nanotube/Polymer Composites by Shear Mixing. 2001. Available online: https://acs.omnibooksonline.com/data/papers/2001_37.3.pdf (accessed on 30 November 2018).
31. Charitidis, C.A. Nanomechanical and nanotribological properties of carbonbased thin films: A review. *J. Refract. Met. Hard Mater.* **2010**, *28*, 51–70. [[CrossRef](#)]
32. Koumoulos, E.P.; Charitidis, C.A.; Papageorgiou, D.P.; Papathanasiou, A.G.; Boudouvis, A.G. Nanomechanical and Nanotribological Properties of Hydrophobic Fluorocarbon Dielectric Coating on Tetraethoxysilane for Electrowetting Applications. *Surf. Coat. Technol.* **2012**, *206*, 3823–3831. [[CrossRef](#)]
33. Oliver, W.C.; Pharr, G.M. An improved technique for determining hardness and elastic modulus using load and displacement sensing indentation experiments. *Mater. Res.* **1992**, *7*, 1564–1583. [[CrossRef](#)]
34. Sneddon, I.N. Boussinesq's problem for a rigid cone. *Math. Proc. Camb. Philos. Soc.* **1948**, *44*, 492–507. [[CrossRef](#)]
35. King, R.B. Elastic analysis of some punch problems for a layered medium. *Int. J. Solids Struct.* **1987**, *23*, 1657–1664. [[CrossRef](#)]
36. Bei, H.; George, E.P.; Hay, J.L.; Pharr, G.M. Influence of Indenter Tip Geometry on Elastic Deformation during Nanoindentation. *Phys. Rev. Lett.* **2005**, *95*, 045501. [[CrossRef](#)]
37. Kim, H.; Bae, H.; Yu, J.; Kima, S. Thermal conductivity of polymer composites with the geometrical characteristics of graphene nanoplatelets. *Sci. Rep.* **2016**, *6*, 26825. [[CrossRef](#)]
38. Bellucci, S.; Balasubramanian, C.; Micciulla, F.; Rinaldi, G. CNT composites for aerospace applications. *J. Exp. Nanosci.* **2007**, *2*, 193–206. [[CrossRef](#)]
39. Psarras, G. Charge transport properties in carbon black/polymer composites. *J. Polym. Sci. Part B* **2007**, *45*, 2535–2545. [[CrossRef](#)]
40. Psarras, G. Conductivity and dielectric characterization of polymer nanocomposites. In *Polymer Nanocomposites: Physical Properties and Applications*; Woodhead Publishing Limited: Cambridge, UK, 2010; pp. 31–69.
41. Pontikopoulos, P.; Psarras, G. Dynamic percolation and dielectric response in multiwall carbon nanotubes/poly(ethylene oxide) composites. *SAM* **2013**, *5*, 1420. [[CrossRef](#)]
42. Saito, S.; Sasabe, H.; Nakajima, T.; Yada, K. Dielectric relaxation and electrical conduction of polymers as a function of pressure and temperature. *J. Polym. Sci. A2* **1968**, *6*, 1297. [[CrossRef](#)]
43. Xu, F.; Sun, L.X.; Zhang, J.; Qi, Y.N.; Yang, L.N.; Ru, H.Y.; Wang, C.Y.; Meng, X.; Lan, X.F.; Jiao, Q.Z.; et al. Thermal stability of carbon nanotubes. *J. Therm. Anal. Calorim.* **2010**, *102*, 785–791. [[CrossRef](#)]
44. Si Eun, L.; Seho, C.; YoungSeak, K. Mechanical and thermal properties of MWCNT reinforced epoxy nanocomposites by vacuum assisted resin transfer molding. *Carbon Lett.* **2014**, *15*, 32–37.
45. Baldissera, A.F.; de Miranda, K.L.; Bressy, C.; Martin, C.; Margailan, A.; Ferreira, C.A. Using Conducting Polymers as Active Agents for Marine Antifouling Paints. *Mater. Res.* **2015**, *18*, 1129–1139. [[CrossRef](#)]
46. Koumoulos, E.P.; Charitidis, C.A.; Daniolos, N.M.; Pantelis, D.I. Nanomechanical properties of friction stir welded AA6082T6 aluminum alloy. *Mater. Sci. Eng. B* **2011**, *176*, 1585–1589. [[CrossRef](#)]
47. Li, Y.; Yu, T.; Pui, T.; Chen, P.; Zheng, L.; Liao, K. Fabrication and characterization of recyclable carbon nanotube/polyvinyl butyral composite fiber. *Compos. Sci. Technol.* **2011**, *71*, 1665–1670. [[CrossRef](#)]

48. Zhuang, G.S.; Sui, G.X.; Sun, Z.S.; Yang, R. Pseudoreinforcement effect of multiwalled carbon nanotubes in epoxy matrix composites. *J. Appl. Polym. Sci.* **2006**, *102*, 3664–3672. [[CrossRef](#)]
49. Fiedler, B.; Gojny, F.H.; Wichmann, M.H.; Nolte, M.C.; Schulte, K. Fundamental aspects of nanoreinforced composites. *Compos. Sci. Technol.* **2006**, *66*, 3115–3125. [[CrossRef](#)]
50. Cheng, Y.T.; Cheng, C.M. What is indentation hardness? *Surf. Coat. Technol.* **2000**, *133–134*, 417–424. [[CrossRef](#)]
51. Leyland, A.; Matthews, A. Design criteria for wear resistant nanostructured and glassy metal coatings. *Surf. Coat. Technol.* **2004**, *177–178*, 317–324. [[CrossRef](#)]
52. Leyland, A.; Matthews, A. Optimization of Nanostructured Tribological Coatings. In *Nanostructured Coatings*; Springer: New York, NY, USA, 2007.



© 2019 by the authors. Licensee MDPI, Basel, Switzerland. This article is an open access article distributed under the terms and conditions of the Creative Commons Attribution (CC BY) license (<http://creativecommons.org/licenses/by/4.0/>).